electronic materials

MDPI

Article

One-Step Cost-Effective Growth of High-Quality Epitaxial Ge Films on Si (100) Using a Simplified PECVD Reactor

Jignesh Vanjaria [1], Venkat Hariharan [2], Arul Chakkaravarthi Arjunan [3,*], Yanze Wu [4], Gary S. Tompa [3] and Hongbin Yu [4]

1 School for Engineering of Matter, Transport and Energy, Arizona State University, Tempe, AZ 85281, USA; jvanjari@asu.edu
2 Logic Technology Development, Intel Corporation, Hillsboro, OR 97124, USA; venkat.hariharan@intel.com
3 Structured Materials Industries Inc., Piscataway, NJ 08854, USA; gstompa@gmail.com
4 School for Electrical, Computer and Energy Engineering, Arizona State University, Tempe, AZ 85281, USA; yanzewu@asu.edu (Y.W.); Hongbin.Yu@asu.edu (H.Y.)
* Correspondence: aarul.smi@gmail.com

Abstract: Heteroepitaxial growth of Ge films on Si is necessary for the progress of integrated Si photonics technology. In this work, an in-house assembled plasma enhanced chemical vapor deposition reactor was used to grow high quality epitaxial Ge films on Si (100) substrates. Low economic and thermal budget were accomplished by the avoidance of ultra-high vacuum conditions or high temperature substrate pre-deposition bake for the process. Films were deposited with and without plasma assistance using germane (GeH_4) precursor in a single step at process temperatures of 350–385 °C and chamber pressures of 1–10 Torr at various precursor flow rates. Film growth was realized at high ambient chamber pressures (>10^{-6} Torr) by utilizing a rigorous ex situ substrate cleaning process, closely controlling substrate loading times, chamber pumping and the dead-time prior to the initiation of film growth. Plasma allowed for higher film deposition rates at lower processing temperatures. An epitaxial growth was confirmed by X-Ray diffraction studies, while crystalline quality of the films was verified by X-ray rocking curve, Raman spectroscopy, transmission electron microscopy and infra-red spectroscopy.

Keywords: epitaxial growth; germanium; plasma enhanced chemical vapor deposition

Citation: Vanjaria, J.; Hariharan, V.; Arjunan, A.C.; Wu, Y.; Tompa, G.S.; Yu, H. One-Step Cost-Effective Growth of High-Quality Epitaxial Ge Films on Si (100) Using a Simplified PECVD Reactor. *Electron. Mater.* **2021**, 2, 482–494. https://doi.org/10.3390/electronicmat2040033

Academic Editor: Wojciech Pisula

Received: 29 August 2021
Accepted: 7 October 2021
Published: 10 October 2021

1. Introduction

Germanium has played a crucial role as a semimetal for its attributes to enable electronic–photonic integration with silicon [1]. Germanium is superior to silicon in several properties, including higher carrier mobility than Si, a smaller delta between the Γ point and the L/X point of 136 meV, and longer cut-off wavelength than Si (at 1.55 μm) [2,3]. Germanium thin films find applications in waveguides in integrated photonic circuits [4,5]. Ge thin films also act as buffers for the growth of group IV alloys such as GeSn and SiGeSn on Si substrates to counter the issue of the large lattice mismatch between the alloys and Si substrate [6]. These group IV alloys can then be bandgap and lattice engineered by varying their atomic compositions to achieve active photonic components such as light emitting diodes, lasers, and detectors [7]. The addition of a thin hydrogenated Ge layer was also seen to enable carbon-doped a-Si:H solar cells by the avoidance of the drop in the fill factor (FF) and the elimination of the Schottky barrier [8]. This resulted in a 25% efficiency enhancement for the a-Si:H solar cells in presence of the a-Ge:H interfacial buffer. For these reasons, the hetero-epitaxial growth of Ge on Si has been studied extensively in the last two decades.

Molecular beam epitaxy (MBE) and ultra-high vacuum chemical vapor deposition (UHV-CVD) [9] are among the most widely adopted techniques for Ge epi growth. However, these techniques involve expensive reactors, cryogenic pumps, and/or complicated

unit-processes [10,11]. These enable chamber background pressures of $<10^{-8}$ Torr. Such low chamber pressures are essential to ensure partial pressures of oxygen and water vapor in the chamber are lower than the critical value to ensure the Si substrate surface is not oxidized. Additionally, such techniques involve the use of exotic precursors (like higher-order hydrides), two step low-temperatures/high-temperature (LT/HT) growth and high temperature annealing to attain high film growth rates and low defect densities in the films [12,13]. Hence, they result in a high thermal budget, and therefore the cost of fabrication. The high temperatures involved have the potential to adversely affect films with low thermal budgets used in the device process flows [14]. A low temperature single step deposition process solves these challenges as it leads to significant cost reduction and limits the thermal strain arising from the difference in thermal coefficients of expansion between Ge and Si [15]. For the aforesaid reasons, Ge film growth at relatively lower temperatures (<400 °C) were studied in this work.

Plasma enhanced chemical vapor deposition is being extensively used in the industry to grow a wide variety of thin films for solar cells and photovoltaics such as hydrogenated silicon nitride (SiN_x) and aluminum oxide (AlO_x), intrinsic and doped amorphous silicon (a-Si), etc. [16]. Industrial PECVD reactors deploy either direct or remote systems. The substrates are placed between two parallel plates in direct contact with the electrodes and the excited plasma for the former, while the opposite holds true for the latter [17]. Radio-frequency (RF) discharge-based PECVD utilizes the capacitive coupling between the electrodes, which excites the precursor gases, induces a chemical reaction, and results in the deposition of the reaction products [18]. PECVD is known to provide a higher film deposition rate compared to conventional CVD through the interaction of the precursor sources with the highly energetic ions and radicals generated in the plasma [13,15,19]. In this work, Ge films were deposited using an in-house assembled simplified RF PECVD reactor by the use of the substrate–electrode direct-contact approach described above.

2. Experimental

A. Apparatus: The assembly consisted of a cylindrical quartz growth chamber with an industrial showerhead system (for uniform precursor gas delivery) at the top and a vacuum system (employing a turbomolecular pump and a mechanical pump) at the bottom connected through flanges. Germane (GeH_4) was chosen as the Ge precursor for film growth, as it is the most commercially available and the most economical precursor for Ge film growth [20]. The need for ultra-high vacuum conditions during film growth was circumvented by the deployment of an ex situ chemical cleaning procedure comprising of HF solution and H_2SO_4-H_2O_2 solution baths to etch away the native oxide and get a hydrogen-terminated surface [17]. Thus, high quality films were deposited at a relatively higher chamber background pressure ($>10^{-6}$ Torr) and background oxygen. The experimental details and the results from film characterization are provided in the upcoming sections.

B. Coupon preparation: Lightly n-doped (phosphorous) Si (100) wafers (resistivity, ρ = 4–16 Ωcm) were used as templates for Ge growth. The samples were diced into 1 cm × 1 cm coupons for the runs. The cleaning procedure employed in the study was adopted from Carroll et al. (2000) to etch away native oxide from the coupons [21]. This procedure enabled the avoidance of an in situ pre-deposition H_2 bake process. Firstly, the coupons were washed by acetone, isopropyl alcohol (IPA), and DI water for the removal of organic residues. Then, a 1:100 HF (50% In DI water) aqueous solution bath was used for native oxide etch. The metal contaminants were removed from the substrate using a bath of H_2SO_4:H_2O_2 (35%) 1:1 ratio at 70 °C for about 20 min. The coupons were then re-introduced to the HF bath for 20 min to remove the oxide formed by H_2O_2 and render H-terminated surfaces. The coupons were then rinsed with DI water, dried with a nitrogen gun, and instantaneously transferred to the PECVD chamber.

C. Ge epi-growth: The in-house assembled reactor as shown in the schematic (Figure 1) was comprised of a tubular chamber made of quartz, a gas flow-control and delivery

system, and a vacuum system with a series of mechanical pumps and a turbomolecular pump connected by flanges. The cleaned Si coupons were placed on a molybdenum (Mo) susceptor inside the reactor, the flanges were screwed, and the chamber was pumped down using a mechanical pump. Higher levels of vacuum were created by means of a turbomolecular pump which was operated for about ~20 min. A combination gage was used to measure the vacuum levels. Once the turbomolecular pump was able to establish the target levels of ~10^{-5} torr, it was disconnected by valves and a rotary pump was used to maintain the target levels with a blower pump in series over the course of the epi growth runs. H_2 gas flowed into the chamber, and a throttle valve was used to attain the desired pressures. Induction coils were used to heat the Mo susceptor to toggle coupon temperatures. The induction heating method ensured that the chamber walls stayed cold, which was necessary to limit gas-phase reactions to the surface of the substrate. The H_2 flow also ensured that the gases generated from the side walls of the quartz chamber are pushed down into the vacuum system, and thus avoided contamination of the Si coupons. The temperature of the Si coupons was measured by means of an Optris pyrometer suited for the range of 300–800 °C. The input current on the induction coil was modulated to toggle the Si coupon temperatures between the runs. On achieving the desired temperatures, a showerhead was used to inject GeH_4 gas (10% in Ar) to minimize concentration gradients across the radius of the chamber, which aided with uniformity in deposition. Hydrogen was used as a carrier gas and the partial pressure of the precursor was varied as required by changing the precursor flow rate rates. Plasma was generated in the chamber during film growth using RF plasma induction coil placed between injection and susceptor powered by a 250 kHz 1 kW RF power supply. The reactor pressure was controlled by a throttle valve. Ge films were deposited at substrate temperatures of 350 °C and 385 °C. The chamber pressures were varied between 1 and 10 torr. GeH_4 precursor flow rates of 20–160 sccm were studied. Films were deposited with and without plasma assistance. GeH_4 in Ar precursor flowed for 60 min for each experiment. At the end of each run, GeH_4 in Ar gas was disconnected and H_2 gas flowed through the quartz chamber to cool down the surface of the Si coupons. The film growth conditions for different attempted runs are summarized in Table 1.

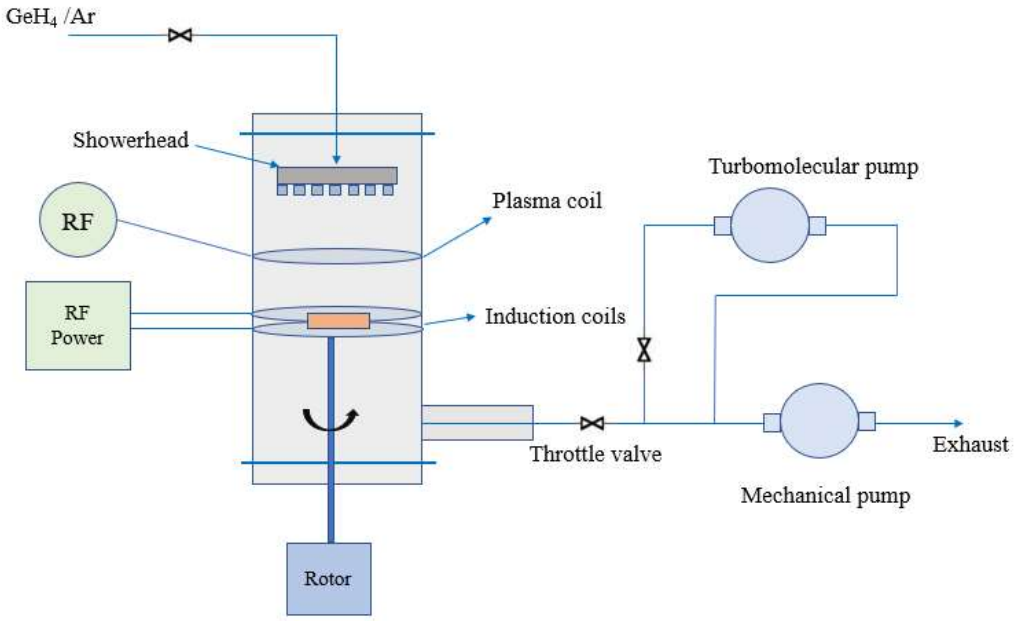

Figure 1. Schematic diagram of the simplified PECVD reactor used for deposition of the Ge thin films.

Table 1. Film growth conditions for different runs.

Run No.	Substrate Temperature (°C)	Chamber Pressure (Torr)	GeH_4 Flow Rate (sccm) (GeH_4 Partial Pressure (mTorr))	Plasma Enhancement
1	385	1	20 (4)	No
2	385	10	20 (4)	No
3	385	10	80 (16)	No
4	385	10	160 (32)	No
5	350	1	20 (4)	No
6	350	10	20 (4)	No
7	350	10	80 (16)	No
8	350	10	160 (32)	No
9	350	1	20 (4)	Yes
10	350	10	20 (4)	Yes
11	350	10	80 (16)	Yes
12	350	10	160 (32)	Yes

D. Epi-film Characterization: The structural properties and deposition rates of the Ge epi films were studied using X-ray diffraction (XRD), scanning electron microscopy (SEM), and transmission electron microscopy (TEM), and their optical properties were characterized by Raman spectroscopy and infra-red (IR) spectroscopy. The film structure and quality were characterized using XRD spectra and X-ray rocking curves, using PANalytical XPert Pro MRD diffractometer with Cu Kα radiation. X-section SEM images of the films were captured using a Hitachi S-4700-II SEM tool and were used to calculate the thicknesses of the obtained films. Raman spectroscopy measurements were performed by a 532 nm 50 mW green laser beam coupled to a WiTec Alpha300R Confocal Raman Imaging system. The strain present in the films were analyzed by a Princeton Instruments Acton SP2300 imaging spectrograph. Infrared spectroscopy (IR) runs were carried out at room temperature using a Perkin Lambda 950 UV/Vis/NIR spectrometer for the wavelength range of 1500–2200 nm for film absorbance characteristics. Transmission Electron Microscopy was performed using a Philips CM200-FEG high resolution TEM at an accelerating voltage of 200 kV to analyze crystalline structure and defects in the films. Surface height maps and roughness were measured using a Zygo ZeGage 3D optical surface profile at 20× magnification.

3. Results and Discussion

It was seen that runs 1 and 5 at substrate temperatures of 385 °C and 350 °C, respectively, with chamber pressure = 1 torr did not result in film deposition. Increasing the chamber pressure to 10 torr led to film deposition. This observation is explained by the concept of mean free path, which is the average distance that the precursor molecules travel before colliding with other molecules [22,23]. The mean free path, λ, is given by

$$\lambda = \frac{kT}{\sqrt{2} * \pi * d^2 * P}$$

where k is the Boltzmann constant = 1.38×10^{-23} $m^2 kg\ s^{-2} K^{-1}$;

d is the effective diameter of the molecules (in the order of 1 nm);

T is the temperature of the chamber (K);

P is the chamber pressure (Pa).

By estimating the chamber temperature to be 523 K and diameter to be ~1 nm, it was observed that the mean free path at 1 torr is ~1.22 um and that at 10 torr is ~0.122 um. The higher pressure should thus result in a much higher probability of collisions between the precursor gas molecules causing more dissociation and hence resulting in film deposition. Higher pressure would also lead to higher residence time at the substrate surface.

X-ray diffraction spectra of the films (collected between 2θ of 20° and 75°) confirmed that all the films have been deposited in an epitaxial manner irrespective of the high chamber background pressure (>10^{-6} torr). This was achieved through the optimization of the process steps and process times before initiating film growth. The use of turbo pumping substantially reduced the concentration of oxygen and water vapor during the onset of the crystal growth. The turbo pump was used to achieve a background pressure of ~5 × 10^{-5} torr. Thus, the partial pressure of oxygen in the background after pumping was 8 × 10^{-6} torr (20% of atmosphere). However, as per Greve (1998), the partial pressure of oxygen needs to be below 1.94 × 10^{-13} torr at deposition temperature of 385 °C and below 4.69 × 10^{-14} torr at deposition temperature of 350 °C [23]. The value of oxygen partial pressure during the process was therefore much higher than the required values. To overcome this, the silicon substrate surface was terminated with hydrogen by ex situ cleaning to considerably decrease its' reactivity with oxygen. Additionally, hydrogen flow was maintained continuously after the turbo pumping was stopped and the substrate was only heated to a low temperature (<400 °C). Additionally, the film growth was performed at high Ge/O partial pressure ratios. These steps ensured that the desorption of hydrogen from the surface was inhibited till the first few monolayers of Ge were deposited and consequently allowed the Ge films to be deposited at high background chamber pressures (>10^{-6} Torr) [23–25]. The optimized process flow is shown in Figure 2.

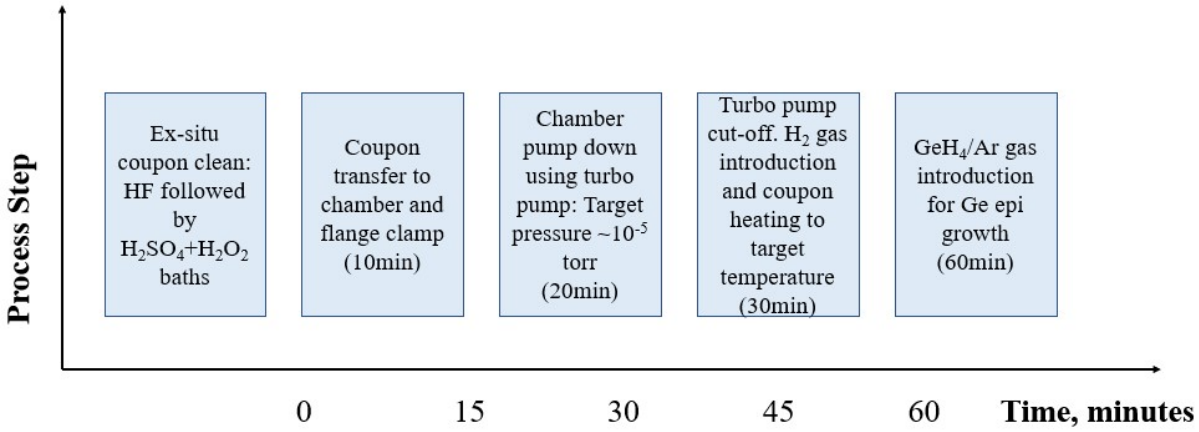

Figure 2. Optimized process flow for deposition of epitaxial Ge films at high background chamber pressure.

Figure 3a shows the impact of GeH_4 partial pressure on the Ge film growth rate at 385 °C and at 350 °C with the chamber pressure maintained at 10 torr. It can be seen that the film growth rate increases with increase in the GeH_4 partial pressure, for both substrate temperatures. This is explained by the higher flux of precursor molecules available for dissociation and deposition at higher partial pressures. The film growth rate is higher at 385 °C than at 350 °C for the same GeH_4 partial pressure. Amongst the factors that determine the growth rate of Ge are the availability of free sites for adsorption of reactant species and the rate of the surface reactions (i.e., dissociation and migration) [25]. With increasing substrate temperature, the coverage of surface by H decreases and the number of sites for adsorption increases [26,27]. Additionally, the higher thermal energy at higher substrate temperature increases the rate of the surface reactions. Thus, the film growth rate increases with increase in temperature. However, at 350 °C, the film growth rate increases linearly with partial pressure while at 385 °C, it increases rapidly initially and then saturates. This is theorized to be due to the GeH_4 decomposition reaction kinetics. This reaction is primarily first order with the reaction rate expressed as:

$$r_{\text{decomposition of } GeH_4} = k * p_{GeH_4}$$

where p_{GeH4} is the partial pressure of GeH_4 in the chamber.

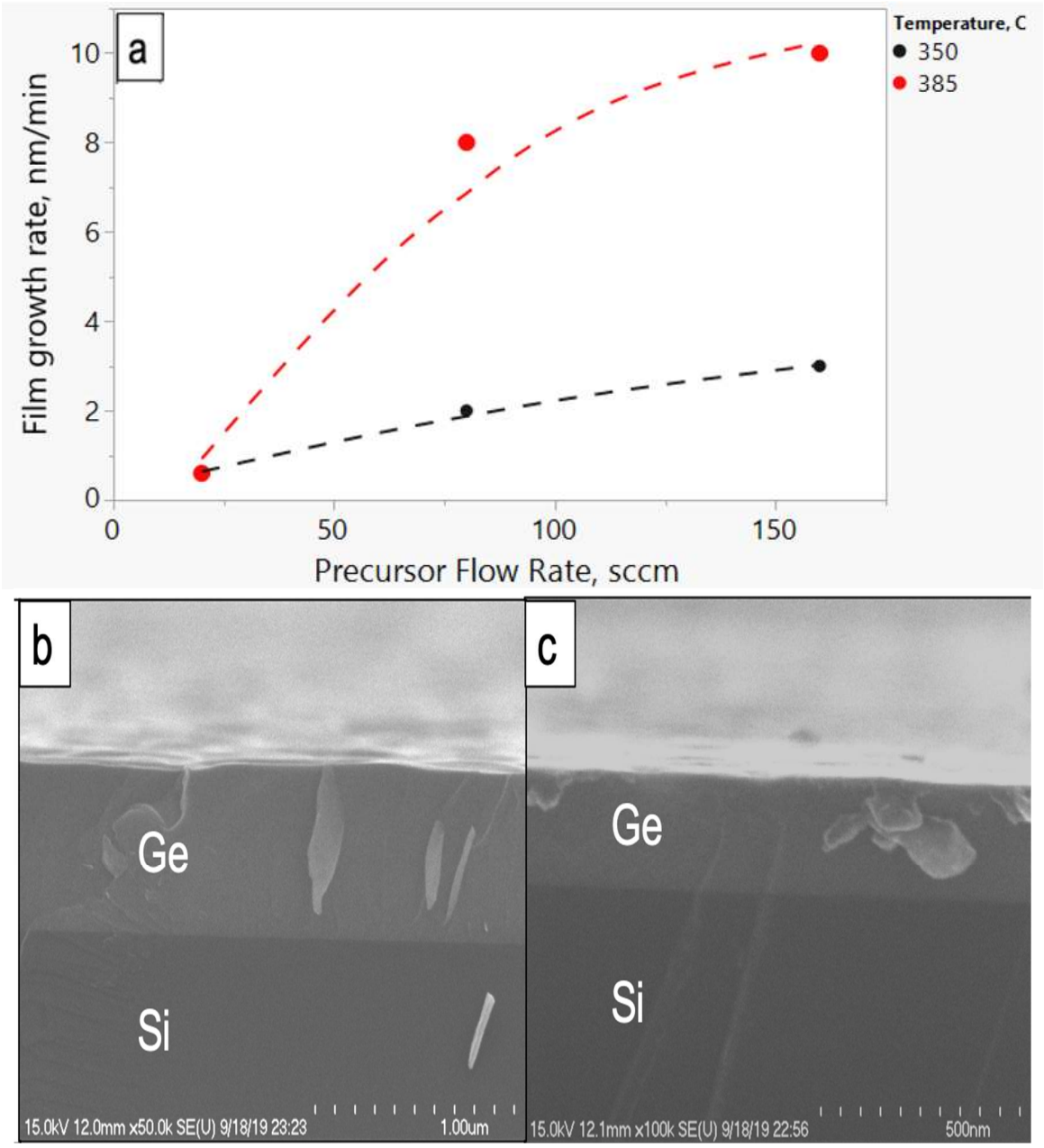

Figure 3. (**a**) Growth rate of Ge films at different GeH_4 partial pressures at chamber pressure of 10 Torr and two different substrate temperatures–350 °C and 385 °C. (**b**) SEM image of the cross section of the Run 4 film. (**c**) SEM image of the cross section of the Run 8 film.

k is the reaction rate constant, which has an exponential relation to temperature expressed by:

$$k = A * e^{\frac{-E_a}{RT}}$$

where A is Arrhenius constant, E_a is the activation energy of decomposition, R is the universal gas constant (8.314 $JK^{-1}mol^{-1}$), and T is the reaction temperature in K.

At the lower substrate temperature and partial pressure, the rate of decomposition is more controlled, and primarily occurs close to the substrate due to the highest temperatures available in that area of the chamber for the reaction to occur. The higher temperature of 385 °C provides a higher volume of reaction sites in the chamber. The higher temperature coupled with high partial pressures of GeH_4 molecules can result in a larger number of collisions at more reaction sites that could result in the deposition of a significant amount

of Ge atoms on the chamber side-walls [28,29]. This explains the dual slope observed for 385 °C in Figure 3a where the deposition rate is seen to be linear at lower partial pressures and tends to attain saturation at higher partial pressures of GeH_4.

Figure 4a shows the film growth rate as a function of GeH_4 partial pressure with plasma enhancement (red) and without plasma enhancement (black). It is seen that the film growth rate is substantially higher with plasma enhancement. This is explained by a higher precursor cracking rate in presence of the plasma. This is due to the kinetic energy provided by the high energy ions and radicals present in the plasma leading to enhanced precursor dissociation [30]. Additionally, the growth rate increases linearly with increase in partial pressure attributed to the lower substrate temperature (i.e., 350 °C), which results in reactions primarily on the substrate and follows first order kinetics as described in the previous section.

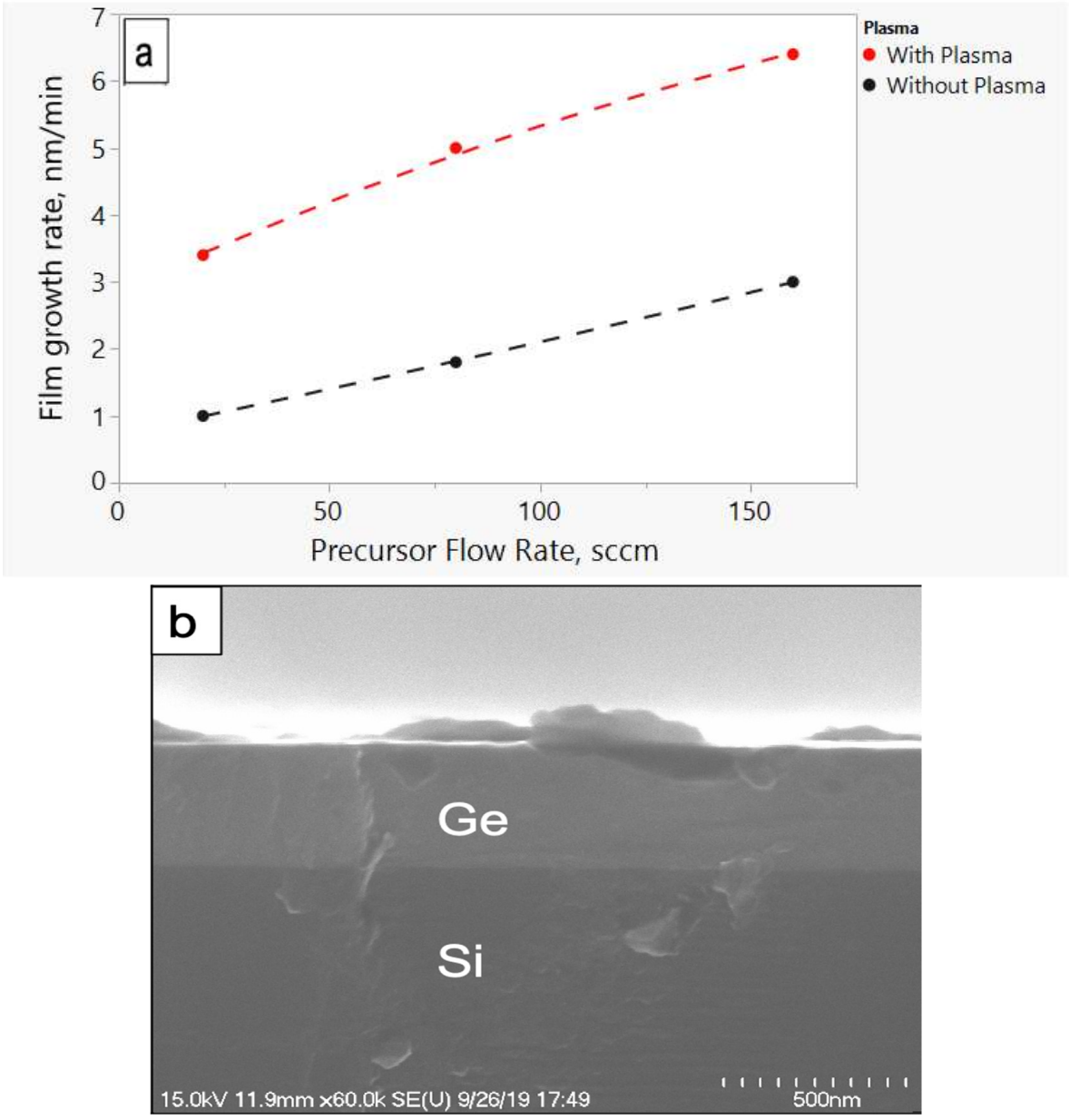

Figure 4. (**a**) Growth rate of Ge films at different GeH_4 partial pressures at chamber pressure of 10 Torr and substrate temperatures 350 °C with and without plasma enhancement. (**b**) SEM image of the cross section of the Run 12 film.

From Figure 5a, it is seen that the full-width half max (FWHM) of the X-ray rocking curves of the films deposited at 385 °C decreases with increasing GeH_4 partial pressure. FWHM of the rocking curve is a measure of the crystalline quality of deposited films: sharper the rocking curve or lower the FWHM, better the crystalline quality [31,32]. This observation implies that higher partial pressures greatly improve the material quality of the films deposited at 385 °C [33]. This is due to the difference in films growth rates obtained under different growth conditions. Lower growth rates would allow for impurities such as background oxygen to incorporate in the depositing film due to the non-UHV CVD conditions [34,35]. This would cause imperfections in the crystal lattice such as point defects and dislocations leading to the degradation of the crystal quality. This phenomenon would be limited at the higher growth rates and would thus result in a film with better crystalline quality. However, for the films deposited with plasma enhancement, the FWHM of the X-ray rocking curves (and thus the material quality) does not change with the change in GeH_4 partial pressure. While the increase in growth rate at the higher partial pressure should restrict the inclusion of background impurities in the films, the bombardment of the crystal lattice from the high energy species present in the plasma could lead to lattice defects (such as broken bonds), and thus result in material quality degradation [11,36,37].

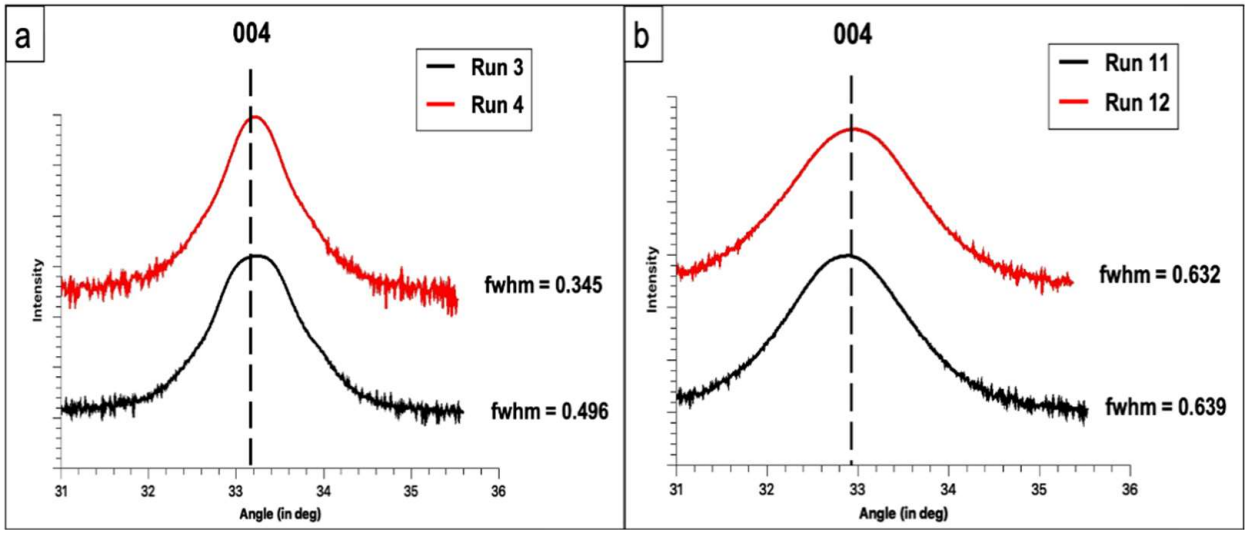

Figure 5. (**a**) X-ray rocking curve of Ge films deposited at 10 torr and different GeH_4 partial pressures at substrate temperature of 385 °C. (**b**) X-ray rocking curve of Ge films deposited at 350 °C with plasma enhancement.

The Raman spectra of the films deposited at low partial pressure (4 mTorr) and high partial pressure (32 mTorr) at different substrate temperatures is shown in Figure 6a. A sharp peak corresponding to the Ge–Ge phonon mode can be seen in all the spectra indicating the high material quality of the films [38]. The strain present in the films can be calculated from the peak shift using the following equation:

$$\varepsilon = \frac{\omega_{\text{Ge–Ge}} - \omega_0^{\text{Ge}}}{b_{\text{Ge–Ge}}} \quad (1)$$

where ε is the strain in the film, $\omega_{\text{Ge–Ge}}$ is the observed Raman peak shift for the Ge–Ge bond, ω_0^{Ge} corresponds to the peak shift for the Ge–Ge bond in bulk Ge, i.e., $\omega_0^{\text{Ge}} = 301$ cm^{-1} and $b_{\text{Ge–Ge}} = -415$ cm^{-1} [39]. The observed peak position and the calculated strain for the films are given in Table 2.

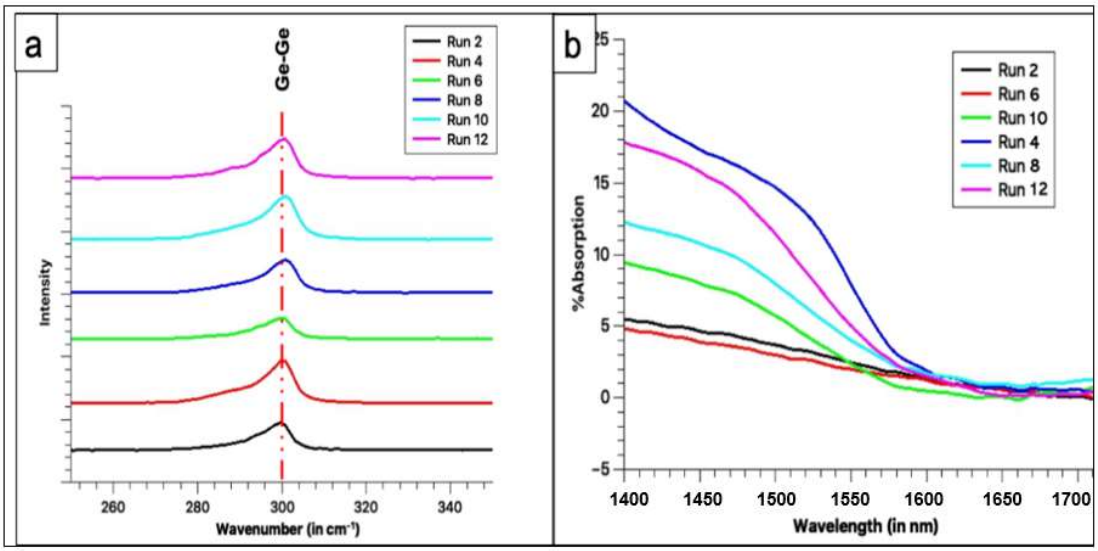

Figure 6. (**a**) Raman spectra of Ge films deposited under various conditions. (**b**) Room temperature IR absorption spectra of Ge films deposited under various conditions.

Table 2. Raman peak positions and calculated strain for Ge films.

Run No.	Film Thickness (nm)	Ge–Ge Peak Position (cm^{-1})	Calculated Strain %
2	75	300.27	0.17
4	600	300.87	0.03
6	60	300.14	0.21
8	200	300.88	0.03
10	210	300.88	0.03
12	400	300.97	0.007

It is noted that the films obtained from runs 2 and 6 have a larger strain present (0.2%), while the remaining films have negligible strain (<0.05%). This is most likely due to the difference in the thickness of the deposited films. The films from runs 2 and 6 have thickness $\leq$ 100 nm, while the remaining films are much thicker. The thicker films relieved the strain arising from the difference in the lattice parameter between Ge and Si substrate through the formation of misfit dislocation at the film-substrate interface, and thus are completely relaxed [36,40]. On the other hand, the films for runs 2 and 6 were not thick enough for strain relief through misfit dislocations and hence show higher %strain as seen with Raman spectroscopy.

Figure 6b shows the absorption spectrum of the films. This was obtained by collecting the reflectance (%R) and transmittance (%T) spectra of the film and then subtracting the sum of the values from 100. It is seen that all the films have a cut-off wavelength of ~1600 nm, which is close to bulk Ge [41]. It can also be seen that the films from runs 2 and 6 have much lower absorption than the remaining films. This can be attributed to the difference in thicknesses of the films as absorbance is directly proportional to the thickness of the films [42]. Films grown by runs 2 and 6 are substantially thinner compared to those grown by the other runs.

Figure 7 shows the dark and bright field TEM images of the epitaxial Ge film deposited in Runs 4, 8 and 12 at different magnifications along with the electron diffraction pattern. As seen from the TEM images, the Ge layer has high crystallinity with periodic atomic arrangement. Some regions in the images have a dark contrast, which is because of the electron clouding process and stress distribution [36]. A high concentration of lattice imperfections, such as dislocations and stacking faults, are concentrated near the interface between the Si substrate and Ge film. Some of the stacking faults (SFs) are observed in the

high magnification TEM image, as marked in Figure 7c,f,i. The stacking faults occur to relieve the strain in the film due to the large lattice mismatch between the Si and Ge and the difference in their coefficients of thermal expansion [36,40]. A clear improvement in the crystalline quality is observed moving away from the interface towards the surface, corresponding to decreasing strain in the lattice. The diffraction patterns confirm the cubic symmetry of the Ge films and the absence of any rings in the pattern confirm the absence of any polycrystalline or amorphous growth.

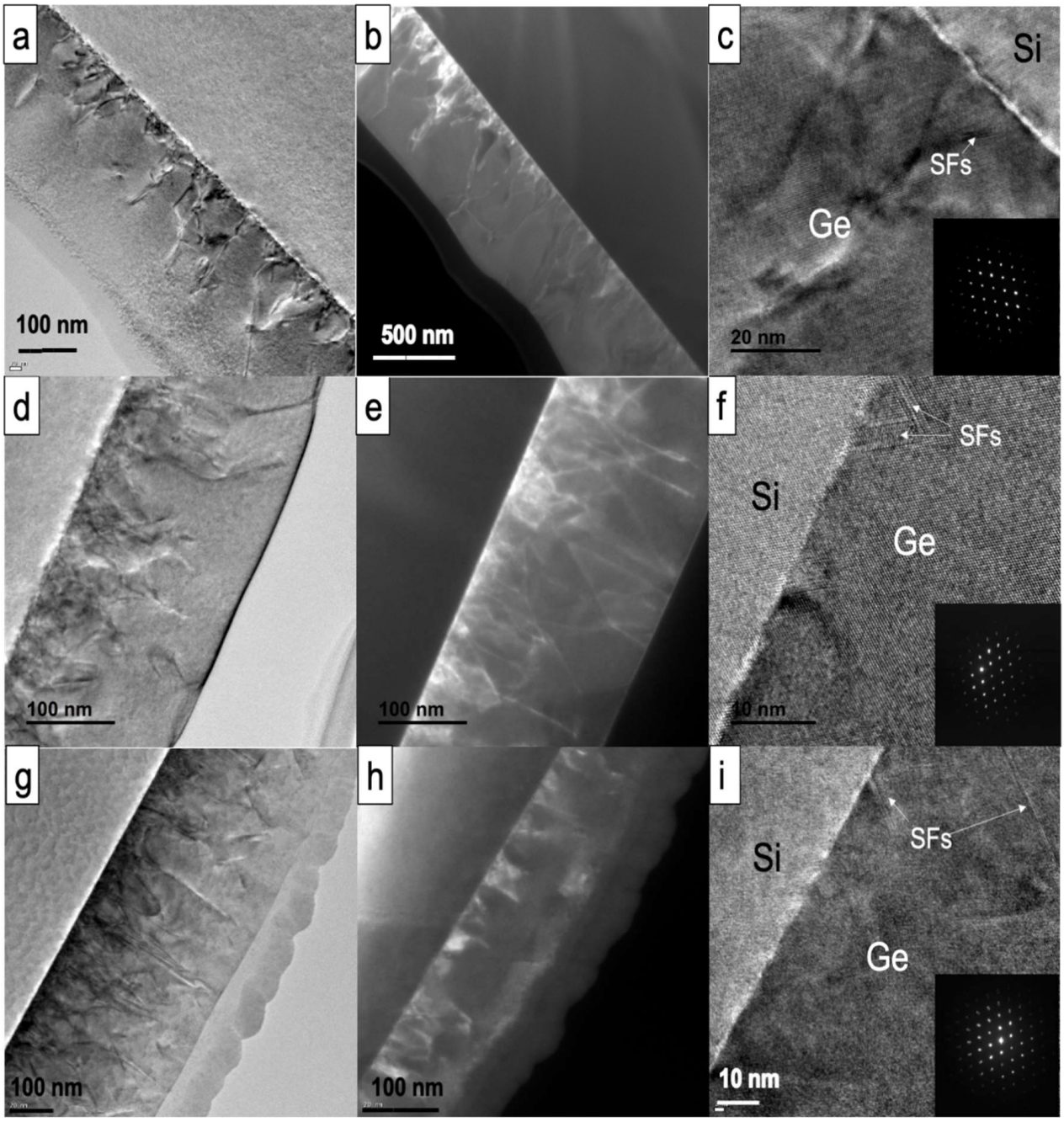

Figure 7. (**a**–**c**) TEM image and diffraction pattern (inset in (**c**)) of Ge film deposited in Run 4. (**d**–**f**) TEM image and diffraction pattern (inset in (**f**)) of Ge film deposited in Run 8. (**g**–**i**) TEM image and diffraction pattern (inset in (**i**)) of Ge film deposited in Run 12. The TEM images confirm the epitaxial growth and good crystalline quality of the deposited films with electron diffraction pattern of the Ge layer showing cubic symmetry.

Figure 8 shows the optical profile of the surface of the films deposited in Runs 4, 8 and 12. The average roughness of the films (Ra) is less than 1 nm in all cases. This shows that the deposited films are highly smooth, which is essential for their application as buffers or waveguides. This further confirms that the films are deposited in a planar manner even with high energy plasma enhancement, and no 3D island growth takes place during film deposition. This is likely because of the low temperatures maintained during film deposition. It is seen that the film from run 4 shows a relatively higher roughness in the nanoscale, which could be attributed to the additional reaction sites on the substrate due to higher H-desorption at the higher temperature of 385 °C, as explained in a prior section.

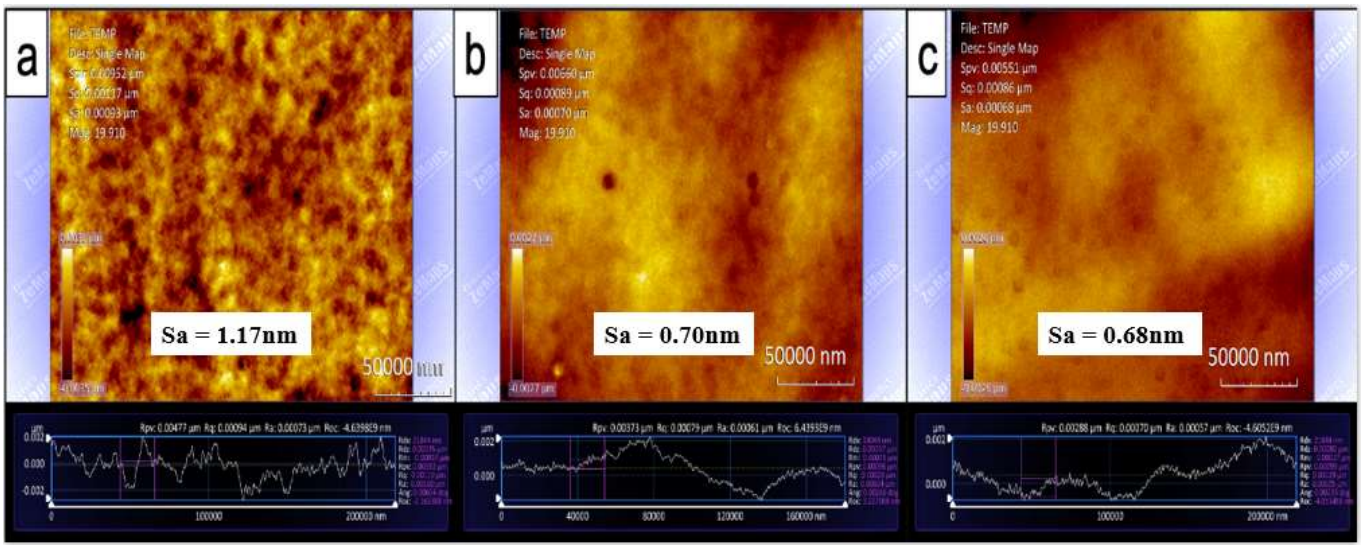

Figure 8. Optical profile of the surface of the Ge films deposited in (**a**) run 4, (**b**) run 8, and (**c**) run 12 showing highly smooth surfaces.

4. Conclusions

A simplified in-house assembled PECVD reactor was used to deposit Ge films epitaxially on Si (100) substrates. Films were deposited at low substrate temperatures (350–385 °C) and low chamber pressure (10 Torr) using GeH_4 as Ge precursor at various precursor partial pressures with and without plasma enhancement. Using a meticulous ex situ substrate cleaning process to get a hydrogen terminated surface, optimizing times for wafer loading, chamber pumping using turbomolecular pump and commencement of film deposition and low temperature growth (<400 °C) allowed heteroepitaxial growth of Ge films at high chamber background pressures (>10^{-6} Torr). Thus, a low economic and thermal budget technology to deposit Ge films epitaxially on Si was successfully realized. The high crystalline quality of the obtained films was confirmed by X-ray rocking curve analysis and optical characterization. Plasma enhancement was shown to result in a higher rate of film deposition (2–3 times higher), and thus can be coupled with the use of low growth temperatures. Growth rate was also found to increase with an increase in the substrate temperature and precursor partial pressure. Improvement in the film material quality was observed with increasing GeH_4 partial pressure due to higher growth rates. Strain in the films was shown to be dependent on the film thickness, with fully relaxed Ge films achieved for film thicknesses $\geq$ 200 nm. The process reported in this work can be used to deposit epitaxial Ge films and possibly other Group IV materials in a cost-effective way.

Author Contributions: J.V.: Conception, analysis, and writing, V.H.: Conception, analysis, and writing, Y.W.: Characterization support, A.C.A.: Conception, analysis, and writing, G.S.T. and H.Y.: Conception. All authors have read and agreed to the published version of the manuscript.

Funding: The research was funded by US-Department of Energy, NASA, Arizona State University and National Science Foundation. US-Department of Energy (#DOE-STTR-DE-SC0015164) for project funding; NASA (STTR Contract#80NSSC18P2145.STTR-2018-I for project funding; Eyring Materials Center for X-ray diffraction and NIR spectroscopy facilities; Center for Solid State Electronics Research Electron Microscopy lab at Arizona State University; Qing Hua Wang for Raman spectroscopy and National Science Foundation (grant nos. 1624842, 1839485, 1933742).

Institutional Review Board Statement: Not applicable.

Informed Consent Statement: Not applicable.

Data Availability Statement: The data underlying this article will be shared on reasonable request from the corresponding author.

Conflicts of Interest: The authors declare no conflict of interest.

References

1. Ye, H.; Yu, J. Germanium epitaxy on silicon. *Sci. Technol. Adv. Mater.* **2014**, *15*, 024601. [CrossRef] [PubMed]
2. Lee, K.H.; Bao, S.; Lin, Y.; Li, W.; Anantha, P.; Zhang, L.; Wang, Y.; Michel, J.; Fitzgerald, E.A.; Tan, C.S. Hetero-epitaxy of high quality germanium film on silicon substrate for optoelectronic integrated circuit applications. *J. Mater. Res.* **2017**, *32*, 4025–4040. [CrossRef]
3. Luo, Y.; Zheng, X.; Li, G.; Shubin, I.; Thacker, H.; Yao, J.; Lee, J.-H.; Feng, D.; Fong, J.; Kung, C.-C.; et al. Strong Electro-Absorption in GeSi Epitaxy on Silicon-on-Insulator (SOI). *Micromachines* **2012**, *3*, 345–363. [CrossRef]
4. Chang, Y.-C.; Paeder, V.; Hvozdara, L.; Hartmann, J.-M.; Herzig, H.P. Low-loss germanium strip waveguides on silicon for the mid-infrared. *Opt. Lett.* **2012**, *37*, 2883–2885. [CrossRef] [PubMed]
5. Nedeljkovic, M.; Penadés, J.S.; Mitchell, C.J.; Khokhar, A.Z.; Stankovic, S.; Bucio, T.D.; Littlejohns, C.G.; Gardes, F.Y.; Mashanovich, G.Z. Surface-Grating-Coupled Low-Loss Ge-on-Si Rib Waveguides and Multimode Interferometers. *IEEE Photonics Technol. Lett.* **2015**, *27*, 1040–1043. [CrossRef]
6. Khazaka, R.; Aubin, J.; Nolot, E.; Hartmann, J.M. Investigation of the Growth of Si-Ge-Sn Pseudomorphic Layers on 200 mm Ge Virtual Substrates: Impact of Growth Pressure, HCl and Si2H6 Flows. *ECS Trans.* **2018**, *86*, 207–218. [CrossRef]
7. Xu, C.; Senaratne, C.L.; Kouvetakis, J.; Menéndez, J. Compositional dependence of optical interband transition energies in GeSn and GeSiSn alloys. *Solid-State Electron.* **2015**, *110*, 76–82. [CrossRef]
8. Kim, J.; Abou-Kandil, A.I.; Hong, A.J.; Saad, M.M.; Sadana, D.K.; Chen, T.-C. Efficiency enhancement of a-Si:H single junction solar cells by a-Ge:H incorporation at the p+ a-SiC:H/transparent conducting oxide interface. *Appl. Phys. Lett.* **2011**, *99*, 062102. [CrossRef]
9. Wirths, S.; Buca, D.; Mussler, G.; Tiedemann, A.T.; Holländer, B.; Bernardy, P.; Stoica, T.; Grützmacher, D.; Mantl, S. Reduced Pressure CVD Growth of Ge and Ge1−xSnx Alloys. *ECS J. Solid State Sci. Technol.* **2013**, *2*, N99–N102. [CrossRef]
10. Hartmann, J.-M.; Grampeix, H.; Clavelier, L. Epitaxial Growth of Ge Thick Layers on Nominal and 6oC off Si(001); Ge Surface Passivation by Si. *ECS Trans.* **2009**, *16*, 583–590. [CrossRef]
11. Alharthi, B.; Grant, J.M.; Dou, W.; Grant, P.C.; Mosleh, A.; Mortazavi, M.; Li, B.; Naseem, H.; Yu, S.-Q.; Du, W. Heteroepitaxial Growth of Germanium-on-Silicon Using Ultrahigh-Vacuum Chemical Vapor Deposition with RF Plasma Enhancement. *J. Electron. Mater.* **2018**, *47*, 4561–4570. [CrossRef]
12. Shah, V.; Dobbie, A.; Myronov, M.; Leadley, D. High quality relaxed Ge layers grown directly on a Si(001) substrate. *Solid-State Electron.* **2011**, *62*, 189–194. [CrossRef]
13. Tan, Y.; Tan, C. Growth and characterization of germanium epitaxial film on silicon (001) using reduced pressure chemical vapor deposition. *Thin Solid Films* **2012**, *520*, 2711–2716. [CrossRef]
14. Littlejohns, C.G.; Khokhar, A.Z.; Thomson, D.J.; Hu, Y.; Basset, L.; Reynolds, S.A.; Mashanovich, G.Z.; Reed, G.T.; Gardes, F.Y. Ge-on-Si Plasma-Enhanced Chemical Vapor Deposition for Low-Cost Photodetectors. *IEEE Photonics J.* **2015**, *7*, 1–8. [CrossRef]
15. Cariou, R.; Ruggeri, R.; Tan, X.; Mannino, G.; Nassar, J.; Cabarrocas, P.R.I. Structural properties of relaxed thin film germanium layers grown by low temperature RF-PECVD epitaxy on Si and Ge (100) substrates. *AIP Adv.* **2014**, *4*, 77103. [CrossRef]
16. Boentoro, T.W.; Szyszka, B. *Protective Coatings for Optical Surfaces, Optical Thin Films and Coatings: From Materials to Applications*; Woodhead Publishing Series in Electronic and Optical Materials; Woodhead Publishing: Sawston, UK, 2013; pp. 540–563.
17. Satpathy, R.; Pamuru, V. *Solar PV Power: Design, Manufacturing and Applications from Sand to Systems*; Academic Press: Cambridge, MA, USA, 2020.
18. Gupta, K.; Jain, N.K.; Laubscher, R. *Advanced Gear Manufacturing and Finishing: Classical and Modern Processes*; Academic Press: Cambridge, MA, USA, 2017.
19. Tian, L.; Fathi, E.; Tarighat, R.S.; Sivoththaman, S. Nanocrystalline silicon deposition at high rate and low temperature from pure silane in a modified ICP-CVD system. *Semicond. Sci. Technol.* **2013**, *28*, 105004. [CrossRef]
20. Mosleh, A.; Alher, M.A.; Cousar, L.C.; Du, W.; Ghetmiri, S.A.; Pham, T.; Grant, J.M.; Sun, G.; Soref, R.A.; Li, B.; et al. Direct Growth of Ge1−xSnx Films on Si Using a Cold-Wall Ultra-High Vacuum Chemical-Vapor-Deposition System. *Front. Mater.* **2015**, *2*, 1–7. [CrossRef]

21. Carroll, M.S.; Sturm, J.C.; Yang, M. Low-Temperature Preparation of Oxygen- and Carbon-Free Silicon and Silicon-Germanium Surfaces for Silicon and Silicon-Germanium Epitaxial Growth by Rapid Thermal Chemical Vapor Deposition. *J. Electrochem. Soc.* **2000**, *147*, 4652–4659. [CrossRef]
22. Asafa, T.B. Influence of Deposition Temperature and Pressure on Structural and Electrical Properties of Boron Doped Poly-Si13Ge87 Films Grown by Chemical Vapor Deposition. *Nanosci. Nanotechnol.* **2013**, *3*, 123–129.
23. Greve, D.W. *UHV/CVD and Related Growth Techniques for Si and Other Materials, Properties of Crystalline Silicon*; Hull, R., Ed.; IET: London, UK, 1999.
24. Suemitsu, M.; Nakazawa, H.; Morita, T.; Miyamoto, N. Observation of Hydrogen-Coverage- and Temperature-Dependent Adsorption Kinetics of Disilane on Si(100) during Si Gas-Source Molecular Beam Epitaxy. *Jpn. J. Appl. Phys.* **1997**, *36*, L625–L628. [CrossRef]
25. Senftleben, O.; Baumgärtner, H.; Eisele, I. Cleaning of Silicon Surfaces for Nanotechnology. *Mater. Sci. Forum* **2008**, *573–574*, 77–117. [CrossRef]
26. Ishii, H.; Takahashi, Y.; Murota, J. Selective Ge deposition on Si using thermal decomposition of GeH4. *Appl. Phys. Lett.* **1985**, *47*, 863–865. [CrossRef]
27. Eres, G.; Sharp, J.W. The role of hydride coverage in surface-limited thin-film growth of epitaxial silicon and germanium. *J. Appl. Phys.* **1993**, *74*, 7241–7250. [CrossRef]
28. Hall, L.H. The Thermal Decomposition of Germane. *J. Electrochem. Soc.* **1972**, *119*, 1593–1596. [CrossRef]
29. Kobayashi, S.-I.; Cheng, M.-L.; Kohlhase, A.; Sato, T.; Murota, J.; Mikoshiba, N. Selective germanium epitaxial growth on silicon using CVD technology with ultra-pure gases. *J. Cryst. Growth* **1990**, *99*, 259–262. [CrossRef]
30. Dou, W.; Alharthi, B.; Grant, P.C.; Grant, J.M.; Mosleh, A.; Tran, H.; Du, W.; Mortazavi, M.; Li, B.; Naseem, H.; et al. Crystalline GeSn growth by plasma enhanced chemical vapor deposition. *Opt. Mater. Express* **2018**, *8*, 3220–3229. [CrossRef]
31. Chaurasia, S.; Raghavan, S.; Avasthi, S. Epitaxial germanium thin films on silicon (100) using two-step process. In Proceedings of the 2016 3rd International Conference on Emerging Electronics (ICEE), Mumbai, India, 27–30 December 2016; pp. 1–4.
32. Ma, Q.-B.; Lieten, R.; Leys, M.; DeGroote, S.; Germain, M.; Borghs, G. Solid phase epitaxy of amorphous Ge films deposited by PECVD. *J. Cryst. Growth* **2011**, *331*, 40–43. [CrossRef]
33. Hartmann, J.; Damlencourt, J.-F.; Bogumilowicz, Y.; Holliger, P.; Rolland, G.; Billon, T. Reduced pressure-chemical vapor deposition of intrinsic and doped Ge layers on Si(001) for microelectronics and optoelectronics purposes. *J. Cryst. Growth* **2005**, *274*, 90–99. [CrossRef]
34. Olubuyide, O.O.; Danielson, D.T.; Kimerling, L.C.; Hoyt, J.L. Impact of seed layer on material quality of epitaxial germanium on silicon deposited by low pressure chemical vapor deposition. *Thin Solid Films* **2006**, *508*, 14–19. [CrossRef]
35. Alharthi, B.; Dou, W.; Grant, P.C.; Grant, J.M.; Morgan, T.; Mosleh, A.; Li, B.; Mortazavi, M.; Naseem, H.; Yu, S.-Q. Low temperature epitaxy of high-quality Ge buffer using plasma enhancement via UHV-CVD system for photonic device applications. *Appl. Surf. Sci.* **2019**, *481*, 246–254. [CrossRef]
36. Kil, Y.-H.; Yuk, S.-H.; Kim, J.H.; Kim, T.S.; Kim, Y.T.; Choi, C.-J.; Shim, K.-H. The low temperature epitaxy of Ge on Si (100) substrate using two different precursors of GeH4 and Ge2H6. *Solid-State Electron.* **2016**, *124*, 35–41. [CrossRef]
37. Grant, P.C.; Dou, W.; Alharthi, B.; Grant, J.M.; Mosleh, A.; Du, W.; Li, B.; Mortazavi, M.; Naseem, H.A.; Yu, S.-Q. Comparison study of the low temperature growth of dilute GeSn and Ge. *J. Vac. Sci. Technol. B* **2017**, *35*, 061204. [CrossRef]
38. Sorianello, V.; Colace, L.; Nardone, M.; Assanto, G. Thermally evaporated single-crystal Germanium on Silicon. *Thin Solid Films* **2011**, *519*, 8037–8040. [CrossRef]
39. Fournier-Lupien, J.-H.; Mukherjee, S.; Wirths, S.; Pippel, E.; Hayazawa, N.; Mussler, G.; Hartmann, J.M.; Desjardins, P.; Buca, D.; Moutanabbir, O. Strain and composition effects on Raman vibrational modes of silicon-germanium-tin ternary alloys. *Appl. Phys. Lett.* **2013**, *103*, 263103. [CrossRef]
40. Luan, H.-C.; Lim, D.R.; Lee, K.K.; Chen, K.M.; Sandland, J.G.; Wada, K.; Kimerling, L.C. High-quality Ge epilayers on Si with low threading-dislocation densities. *Appl. Phys. Lett.* **1999**, *75*, 2909–2911. [CrossRef]
41. Dash, W.C.; Newman, R. Intrinsic Optical Absorption in Single-Crystal Germanium and Silicon at 77oK and 300oK. *Phys. Rev.* **1955**, *99*, 1151–1155. [CrossRef]
42. Aly, S.A.; Akl, A.A. Influence of Film Thickness on Optical Absorption and Energy Gap of Thermally Evaporated Cds0.1se0.9 Thin Films. *Chalcogenide Lett.* **2015**, *12*, 489–496.